Structural Studies on a Protein-Binding Zinc-Finger Domain of Eos Reveal Both Similarities and Differences to Classical Zinc Fingers†

Belinda J. Westman, José Perdomo, Jacqueline M. Matthews, Merlin Crossley, and Joel P. Mackay*

School of Molecular and Microbial Biosciences, University of Sydney, Sydney, New South Wales 2006, Australia

Received March 12, 2004; Revised Manuscript Received July 12, 2004

ABSTRACT: The oligomerization domain that is present at the C terminus of Ikaros-family proteins and the protein Trps-1 is important for the proper regulation of developmental processes such as hematopoiesis. Remarkably, this domain is predicted to contain two classical zinc fingers (ZnFs), domains normally associated with the recognition of nucleic acids. The preference for protein binding by these predicted ZnFs is not well-understood. We have used a range of methods to gain insight into the structure of this domain. Circular dichroism, UV−vis, and NMR experiments carried out on the C-terminal domain of Eos (EosC) revealed that the two putative ZnFs (C1 and C2) are separable, i.e., capable of folding independently in the presence of Zn^{II}. We next determined the structure of EosC2 using NMR spectroscopy, revealing that, although the overall fold of EosC2 is similar to other classical ZnFs, a number of differences exist. For example, the conformation of the C terminus of EosC2 appears to be flexible and may result in a major rearrangement of the zinc ligands. Finally, alanine-scanning mutagenesis was used to identify the residues that are involved in the homo- and hetero-oligomerization of Eos, and these results are discussed in the context of the structure of EosC. These studies provide the first structural insights into how EosC mediates protein−protein interactions and contributes to our understanding of why it does not exhibit high-affinity DNA binding.

There has been substantial interest in zinc-binding domains (zinc fingers or ZnFs) over the last 10 years, because of both their abundance in the human genome and their structural and functional diversity. These small modules are known to bind DNA, RNA, lipids, and other proteins (*1*). Zinc-binding domains are classified according to the number and spacing of zinc-ligating residues, and by far, the most common configuration is the classical or CCHH configuration. Classical ZnFs bind double-stranded DNA in tandem arrays (*2*), and each domain comprises a single N-terminal β hairpin followed an α helix. In contrast to DNA-binding classical ZnFs, protein-binding CCHH ZnFs are poorly characterized. Classical ZnFs from transcriptional regulators such as YY1 and KLF-family proteins have been shown to recruit protein partners in biochemical assays (*3*−*7*), although little else is know about these interactions.

Members of the Ikaros family of proteins (*8*) are predicted to contain two clusters of classical ZnFs (Figure 1). While the N-terminal cluster recognizes specific sequences in double-stranded DNA (*9*−*12*), the C-terminal region has been shown to mediate both homo- and heterotypic interactions with other family members (*8*, *10*, *11*, *13*, *14*). As well as the founding member, the transcriptional regulator Ikaros (*15*), the family also includes Aiolos (*10*), Helios (*12*, *14*),

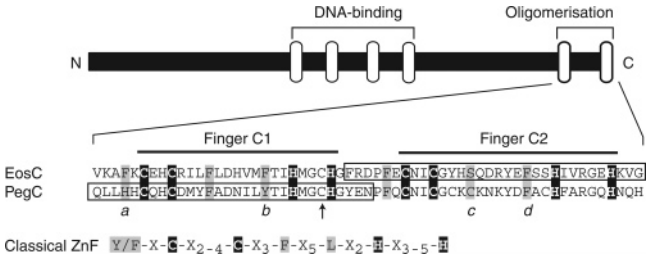

FIGURE 1: Primary structure of Ikaros proteins. A schematic diagram of Ikaros proteins is shown, along with the ZnF domains (white) and the sequences of EosC and PegC. These domains consists of two ZnFs (fingers C1 and C2) that each complies with the consensus sequence of classical ZnFs (shown at the bottom; X refers to any amino acid). The letters a−d indicate differences in EosC and PegC to the consensus sequence. The amino acids that compose the constructs EosC2 and PegC1 are boxed. The arrow shows the position of the putative non-zinc-ligating cysteine residue that was mutated to serine in the constructs EosC1 and PegC1. Zinc-ligating residues and the positions of the conserved hydrophobic residues in classical ZnFs are highlighted in black and gray, respectively.

Eos and Pegasus (*11*, *13*). The mRNA that encodes these proteins is detected primarily in hematopoietic cell lines (*10*−*12*, *14*, *16*−*19*), although Eos mRNA is also expressed in the developing brain and nervous system (*13*) and Pegasus is widely expressed throughout the organism (*11*). Gene-targeting studies in mice have confirmed the central roles of Ikaros and Aiolos in the regulation of hematopoiesis and immunity (*20*−*22*). Interestingly, the protein Trichophinophalangeal syndrome 1 (Trps1), which is otherwise unrelated to Ikaros proteins, contains an Ikaros-like oligomerization domain at its C terminus and has been reported to be present

† This work is supported by grants from the National Health and Medical Research Committee and the University of Sydney Cancer Research Fund. J.M.M. is an ARC Research Fellow. B.J.W. and J.P. were supported by Australian Postgraduate Awards.

* To whom correspondence should be addressed: School of Molecular and Microbial Biosciences, Building G08, University of Sydney, Sydney, NSW 2006, Australia. Phone: +61-2-9351-3906. Fax: +61-2-9351-4726. E-mail: j.mackay@mmb.usyd.edu.au.

10.1021/bi049506a CCC: $27.50
Published on Web 09/29/2004

in the foetal brain (*23*). It has recently been shown that Eos (but not other Ikaros-family proteins) interacts with Trps1 (*24*), and it is possible that these two proteins cooperate in some way to regulate early brain development.

In some instances, the protein−protein interactions mediated by the C-terminal domains of Ikaros proteins facilitate high-affinity DNA binding and concomitant transcriptional regulation (*8*, *10*, *11*, *13*, *14*), consistent with the view that Ikaros-family proteins oligomerize on DNA. While the N-terminal region may contain a variable number of ZnFs arising from alternate splicing (*9*), the C-terminal domain always contains two fingers and is highly conserved, from sea lampreys to humans (*25*, *26*).

Despite the importance of this C-terminal domain in both the biology of Ikaros proteins and, more generally, as a novel protein-recognition domain, nothing is known about its structural characteristics. In this study, the C-terminal domain of Eos (EosC) has been examined using a combination of structural and molecular biological methods. We show that EosC comprises two separable domains that fold in a Zn^{II}-dependent fashion and that both fingers form conformations that resemble classical ZnFs. The solution structure of the second finger of EosC has been determined, and it reveals several unusual properties for a ZnF. Finally, alanine-scanning mutagenesis identified the residues that are involved in the homo-oligomerization of Eos, and these results are discussed in the context of the structure of the C-terminal domain. These data add to our understanding of both the Ikaros proteins and the ability of ZnFs to mediate protein−protein interactions.

EXPERIMENTAL PROCEDURES

Subcloning of Single ZnF Constructs and Mutants Used in Alanine-Scanning Mutagenesis. Single-finger constructs EosC1 (amino acids 474−500; Cys498Ser), EosC2 (amino acids 501−532), PegC1 (amino acids 361−390; Cys385Ser), and EosC (amino acids 474−532; Cys498Ser) were amplified using standard polymerase chain reaction (PCR) techniques. Cysteine substitutions were introduced using site-directed mutagenesis. Mutants (M1−M21) were generated from EosC by either an overlap PCR or a single primer mismatch PCR with *Pfu* polymerase (Stratagene, La Jolla, CA). Primer sequences are available on request.

PegC1 and EosC2 were inserted into pGEX-2T (Amersham Biosciences, NSW, Australia), and EosC1 was inserted into pIH1120 (described previously in ref *24*). For yeast two-hybrid assays, EosC2 and EosC1 were cloned into pGBT9, whereas EosC1 and mutants (M1−M21) were cloned into pGAD10. The DNA encoding M3, M7, M8, and M10 was also inserted into pIH1120.

Overexpression and Purification of Single-Finger Constructs and M3, M7, M8, and M10. PegC1 and EosC2 were produced as C-terminal fusions with glutathione-*S*-transferase (GST), and their overexpression was carried out at 37 °C and induced by the addition of isopropyl-β-D-thiogalactopyranoside (0.1 mM). EosC1, M3, M7, M8, and M10 were overexpressed in a similar manner as C-terminal fusions with maltose-binding protein (MBP), except that glucose (0.2% w/v) was also added to the LB. The subsequent steps (cell lysis, purification by glutathione/amylose-affinity chromatography, and thrombin cleavage) were carried out as previously described (*24*, *27*). A Gly-Ser fragment remained at the N terminus of PegC1 and EosC2 following thrombin cleavage. All single and double ZnF constructs were further purified by C_{18} reversed phase high-pressure liquid chromatography (rpHPLC), and the peptide identities were confirmed using electrospray mass spectrometry.

Circular Dichroism (CD) Spectropolarimetry. Samples were prepared by dissolving lyophilised rpHPLC-purified peptide in 50 μM tris(2-carboxyethyl)phosphine (TCEP; Pierce, Rockford, IL) and 50 μM $ZnSO_4$ to a final concentration of 15 μM. The pH was adjusted to 5.0−6.0 using 1 M NaOH. CD spectra were recorded at 20 °C on a Jasco J-720 spectropolarimeter, equipped with a Neslab RTE-111 temperature controller. CD data were collected over the wavelength range 184−260 nm, with a resolution of 0.5 nm, a bandwidth of 1 nm, and a response time of 1 s using a 1-mm path-length cell. Final spectra were the sum of three scans accumulated at a speed of 20 nm/min and were baseline-corrected.

UV−Vis Spectrophotometry. EosC2 was dissolved in 100 μM TCEP (to 80 μM), and the pH was adjusted to 8.7 using 1 M NaOH. Data were collected at 20 °C on a Shimadzu UV-1601 spectrophotometer using the slow-speed setting. Ultra-violet (250−500 nm) and visible (500−800 nm) spectra were recorded after each addition of a 2.5 mM solution of $CoCl_2$, which was added to both the sample and reference cuvettes. The spectrum for EosC2 without metal was subtracted from all subsequent spectra.

Analytical Ultracentrifugation. Sedimentation equilibrium experiments were carried out at 25 °C using a Beckman Optima XL-A ultracentrifuge equipped with an Anti-60 rotor. The PegC1 NMR sample was examined at two loading concentrations (50 and 100 μM), whereas the EosC2 NMR sample was first dialyzed (with 20 mM CH_3COONa at pH 5.4, 100 mM NaCl, 400 μM TCEP, and 700 μM $ZnSO_4$) and examined at three loading concentrations (50, 100, and 200 μM). Absorbance (280 and 360 nm) versus radius scans (0.001-cm increments) were collected at 3-h intervals until the samples had reached equilibrium. Data were recorded at 45 000 rpm for PegC1 or 45 000 and 54 000 rpm for EosC2. Analysis of the data was carried out using the NONLIN software (*28*). The density of the solvent and the partial specific volume of the peptide (adjusted to include the contribution of Zn^{II}; $p = 0.7187$ g/mL) were estimated using Sednterp (*29*). Final parameters were determined by a nonlinear least-squares fit to models incorporating either a single, nonassociating species or a reversible dimerization reaction. Residuals were examined to determine the goodness of fit.

Sample Preparation for NMR Spectroscopy. PegC1 was dissolved in a solution containing 0.6 mM TCEP and 0.5 mM $ZnSO_4$ to a concentration of ~100 μM. The pH was adjusted to 6.0 by the addition of Na_2HPO_4 (pH 6.0) to a final concentration of 30 mM. EosC2 was resuspended to a final concentration of ~100 μM in a solution containing TCEP and $ZnSO_4$ (100 and 200 μM, respectively). The pH was adjusted to either 5.3 or 6.9, and the sample volume was reduced in a vacuum centrifuge such that the final peptide concentration was ~0.5 mM.

For mixing experiments, lyophilised, rpHPLC-purified EosC1 was resuspended in a 300-μL solution containing TCEP and $ZnSO_4$ (100 and 200 μM, respectively) to a final

concentration of ~40 μM. The pH was adjusted to 5.3. An aliquot of the EosC2 sample was diluted (in MilliQ water) such that its concentration was comparable to the EosC1 sample, as judged by 1D ^{1}H NMR spectra. These two samples were then added together to record the 1D ^{1}H NMR spectrum of the mixture. D_2O (5% v/v; Sigma, St Louis, MO) and 2,2-dimethylsilapentane-5-sulfonic acid (DSS; to 20 μM, Sigma) were added to all NMR samples.

NMR Experiments. NMR spectra were acquired on a Bruker Avance 600 MHz spectrometer and processed and analyzed using XWINNMR (Bruker, Karlsruhe) and XEASY (*30*). Total correlation spectroscopy (TOCSY) spectra were recorded with mixing times of 70 ms, and nuclear Overhauser effect spectroscopy (NOESY) spectra were recorded with mixing times of 250 ms (PegC1) or 200 ms (EosC2). Iterative manual assignment of NOEs was used to calculate initial structures of EosC2 using DYANA (*31*). Initially, the calibration of peak integrals against distance was performed using standard DYANA parameters, and later, the calibration of backbone atoms was reparametrized such that the average distance increased from 3.53 to 4.53 Å. At this stage, the following upper and lower distance restraints were added: Cys507 S^γ−Cys510 S^γ = 3.55−3.95 Å, Cys507 S^γ−His523 $N^{\epsilon 2}$ = 3.30−3.70 Å, Cys507 S^γ−His529 $N^{\epsilon 2}$ = 3.30−3.70 Å, Cys510 S^γ−His523 $N^{\epsilon 2}$ = 3.30−3.70 Å, Cys510 S^γ−His529 $N^{\epsilon 2}$ = 3.55−3.95 Å, and His523 $N^{\epsilon 2}$−His529 $N^{\epsilon 2}$ = 3.30−3.75 Å.

Once no further assignments could be made, further refinement was carried out in an automated manner using ARIA 1.2 (*32*, *33*) implemented in CNS 1.1 (*34*). Zinc coordination (*35*) was incorporated in the ARIA calculations, which were carried out using a standard protocol. The following hydrogen-bond restraints, based on the presence of characteristic α-helical NOE patterns, were included: Arg517 O−Ser521 H^N = 0.50−1.80 Å, Arg517 O−Ser521 N = 0.50−2.8 Å, Tyr518 O−Ser522 H^N = 0.50−1.80 Å, and Tyr518 O−Ser522 N = 0.50−2.80 Å. Final calculations were performed with the φ angles of Arg502 and Ser514 constrained to negative values. The final assignments made by ARIA were checked and corrected manually when necessary. Calculations were carried out in the simplified all-hydrogen PARALLHDG5.2 force field with nonbonded interactions modeled by PROLSQ force field (*36*). Floating chirality assignment (*37*) was used for all methylene and isopropyl groups, because no stereospecific assignments were made. The 20 conformers with the lowest value of E_{tot} were visualized and analyzed using MOLMOL (*38*) and PROCHECK (*39*).

Yeast Two-Hybrid Assays. Competent HF7c yeast cells were transformed simultaneously with the appropriate plasmids using the Clontech Two-Hybrid Matchmaker system protocol (Palo Alto, CA). For the alanine scan, M1−M21 were subcloned into pGAD10 and were cotransformed with either pGBT9-EosC, pGBT9-Ikaros451−517, pGBT9-Pegasus221−420, or pGBT9-Trps1/1222−1281. pGAD10 and pGBT9 encode the Gal4 activation domain and the Gal4 DNA-binding domain, respectively. The transformants were selected on −Leu−Trp minimal media plates after growth at 29 °C and were then patched onto −Leu−Trp−His plates and monitored for growth for up to 3 days.

Homology Modeling and Protein−Protein Docking Using HADDOCK. To model EosC1, Deep View [formerly called Swiss-PdbViewer (*40*, *41*)] was used. The ZnFs with PDB entry codes 1ZNF and 1SP1 were manually loaded as template structures.

For HADDOCK (*42*) calculations, the "active residues" were defined as follows in EosC1: Glu480, His481, Asp488, His489, Val490, Met491, Thr493, and Ile494; and in EosC2: Phe501, Arg502, Asn508, and Ile509. All of these residues also satisfied the requirement of having a high solvent accessibility (>50%), as determined by NACCESS (*43*). The "passive residues" (defined as having a high solvent accessibility and neighboring an active residue) were identified by the manual inspection of structures and were as follows in EosC1: Phe477, Arg483, Leu487, Gly497, and His499; and in EosC2: Asp503, Glu506, His513, and Gly532. Subsets of active and passive residues were used in additional runs. These active and passive residues were converted into ambiguous interaction restraints, with maximum values of 2.0 Å. The flexible interface was defined as all active and passive residues ± two sequential residues, and Gly500 and Phe501 were allowed to be fully flexible. The C terminus of EosC1 and the N terminus of EosC2 were forced to be near each other by including the following unambiguous distance constraint: C of Gly500 (EosC1) − N of Phe501 (EosC2) = 1.0−2.0 Å. The docking procedure was performed using the default parameters supplied with the HADDOCK software, and in the final calculations, 200 structures were generated for rigid-body docking and the 50 lowest-energy structures were used for refinement and analysis. No water refinement was performed.

RESULTS

Selection of C-Terminal Domain Constructs. Earlier work carried out in our laboratory revealed that the C-terminal domain of Eos forms a monodisperse 9−10-subunit oligomer in solution [total molecular mass ~ 70 kDa (*24*)]. Because extensive efforts to crystallize this oligomer were unsuccessful and because classical ZnFs are regarded as autonomously folding motifs, we chose to examine the structural characteristics of each putative ZnF from this region of Eos separately (EosC1 and EosC2; Figure 1). Preliminary work revealed that EosC1 was prone to aggregation, and we therefore instead selected the equivalent ZnF from Pegasus (PegC1) for analysis (the C-terminal domains of Pegasus and Eos exhibit 80% sequence similarity; Figure 1). A third cysteine residue, conserved in the C1 domain of all Ikaros-family proteins and marked with an arrow in Figure 1, was mutated to serine to avoid oxidation problems. This mutation did not affect the ability of the domain to fold in a zinc-dependent fashion. The final constructs used in this study are boxed in Figure 1.

PegC1 and EosC2 Are Separable Domains that Require Zinc(II) to Fold. The far-UV CD spectra of PegC1 (Figure 2) and EosC2 (not shown) were similar when recorded at low pH (~2.0) in the absence of Zn^{II} and were typical of mostly unstructured polypeptides. After the addition of Zn^{II} (to more than 1 molar equiv) and an increase in pH (Figure 2), the observed spectral changes are consistent with the formation of a mixture of both α and β secondary structures in PegC1 and EosC2. Although there are differences in the position of the minima and the wavelength of the zero-crossing point for each polypeptide, it is not straightforward

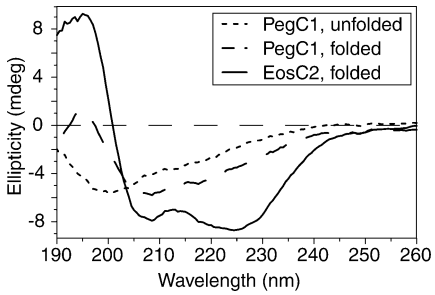

FIGURE 2: CD spectropolarimetry reveals that PegC1 and EosC2 require zinc to fold. In the absence of Zn^{II} and at a low pH, PegC1 and EosC1 (not shown) are mostly unstructured. Upon the addition of Zn^{II} and an increase in pH, PegC1 and EosC2 develop α and β secondary structures. The protein concentration in each sample was ~15 μM, and data were recorded at 20 °C.

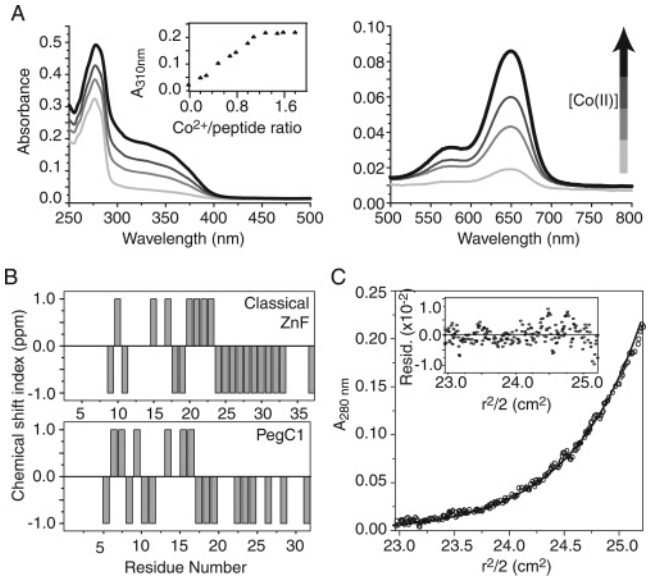

FIGURE 3: PegC1 and EosC2 appear to be classical ZnFs, and EosC2 is monomeric in solution. (A) Position and intensity of peaks in UV (left panel) and visible (right panel) spectra obtained during a Co^{II} titration indicate that EosC2 ligates metal in tetrahedral coordination geometry via two cysteine and two histidine residues. The inset (left panel) shows a plot of absorbance (310 nm) against the Co^{II}/peptide molar ratio, and the appearance of a plateau at the ~1:1 metal/peptide ratio suggests that each EosC2 molecule coordinates one metal ion. (B) Comparison of the H^{α} chemical-shift index against the residue number for the third ZnF from BKLF (top; PDB accession code 1P7A and BMRB accession code 5851) and PegC1 (bottom) is shown. The overall pattern of values for each ZnF suggests that the secondary structure content is similar. (C) Concentration distribution of one data set obtained by sedimentation equilibrium experiments using EosC2 is shown (54 000 rpm, [EosC2] ≈ 200 μM at 20 °C), along with the line of best fit for an ideal, single-species model and the residual plot for this fit (inset).

to draw further conclusions about the relative amounts of secondary structure because of the small size of these domains and the varied number and position of aromatic residues that contribute to the far-UV CD spectrum.

The metal-binding characteristics of EosC2 were also explored by UV−vis spectrophotometry. Co^{II} is often used as a spectroscopic probe for Zn^{II}-binding proteins (*44*, *45*), and Figure 3A shows the spectra obtained as Co^{II} was titrated into EosC2. The charge-transfer bands at ~310 and 340 nm indicate that cysteine residues are involved in metal ligation, while the positions and intensities of bands in the visible region are similar to those obtained for CCHH ZnFs (*44*, *46*). Furthermore, the intensity of these bands ($\epsilon_{650nm} \approx 900$ M^{-1} cm^{-1}) indicates that the coordination of the Co^{II} ion is tetrahedral (*47*). Finally, the change in absorbance at 310 nm (inset, left panel of Figure 3A) reveals that the metal/peptide ratio is probably 1:1. When these results are taken together, they demonstrate that EosC2 ligates one Co^{II} ion via two cysteine and two histidine residues and are consistent with the prediction that EosC2 is a classical ZnF.

PegC1 Resembles a Classical ZnF. Standard ^1H NMR methods were used to assign the proton chemical shifts of PegC1. While the data were not of sufficient quality to allow a full structure determination, we were able to compare the H^{α} chemical shifts with those from a known classical ZnF, namely, the third ZnF of BKLF [PDB accession code 1P7A and BMRB accession code 5851 (*48*)]. A plot of the H^{α} chemical-shift index (*49*) for both peptides reveals similar overall patterns (Figure 3B). Both display a stretch of negative values at the C terminus (indicative of an α helix) and alternating positive and negative values at the N terminus (consistent with the presence of a β hairpin). These results suggest that PegC1 is likely to take up a solution conformation similar to that of a classical ZnF, and because of the high homology within the C terminus of Ikaros-family proteins, it is likely that the structures of this domain from other family members will be very similar. Given that the NMR data for PegC1 indicate that it forms a classical ZnF fold, a homology model was created for EosC1 using Deep View [formerly called Swiss-PdbViewer (*40*, *41*)] and was used for the analysis of results from the alanine scan (see below). In contrast, the quality of the NMR data that we obtained for EosC2 allowed us to determine its structure directly.

Determination of the Structure of EosC2. Analysis of homonuclear two-dimensional NMR experiments permitted the assignment of 80% of the proton chemical shifts in EosC2. Assignments were incomplete for His523, Ile524, Gly527, Glu528, and His529 because of selective spectral broadening (data not shown). Given that sedimentation equilibrium data indicated that EosC2 is monomeric in solution (Figure 3C), the broadening indicated the existence of some form of intramolecular conformational exchange process. To check that this behavior was not a consequence of the pH at which the experiments were conducted, a TOCSY spectrum was recorded on a pH 7.0 sample. The same pattern of selective broadening was observed, and the pH 5.3 data (which were of higher overall quality) were therefore used for the subsequent structural analysis.

After iterative cycles of NOE assignment and structure calculations using DYANA (*31*), the data were used as input into ARIA 1.2 (*32*, *33*) for the final calculation of a family of structures. In addition to NOEs, several other sets of constraints were introduced. A Zn^{II} ion was included, and tetrahedral coordination geometry was maintained. In addition, hydrogen-bond constraints were included for the backbone of residues Arg517−Ser522, because chemical-shift indices in this region (*49*, *50*) indicated the presence of an α helix. ARIA 1.2 identified 534 unambiguous and 15 ambiguous restraints for the final structure calculations (Table 1). The 20 lowest energy structures are presented in Figure 4A. This final ensemble of conformers contains no violations of distance restraints greater than 0.1 Å.

Table 1: Statistics for the Ensembles of EosC2 Structures[a]

Experimental Input	
total NOE restraints	549
total unambiguous restraints	534
intraresidue	288
sequential ($\|i-j\|=1$)	130
medium range ($2 \le \|i-j\| \le 3$)	37
long range ($\|i-j\| \ge 4$)	79
total ambiguous restraints	15
PROCHECK Statistics for First Ensemble (Blue)	
structured region (residues 502−526)	
residues in most favored regions (%)	48.6
residues in allowed regions (%)	32.3
residues in generously allowed regions (%)	15
residues in disallowed regions (%)	4.1
rmsd of backbone atoms (residues 502−526, Å)	0.34 ± 0.16
rmsd of all heavy atoms (residues 502−526, Å)	0.99 ± 0.2
PROCHECK Statistics for Second Ensemble (Orange)	
structured region (residues 502−526)	
residues in most favored regions (%)	41.8
residues in allowed regions (%)	33
residues in generously allowed regions (%)	20.7
residues in disallowed regions (%)	4.6
rmsd of backbone atoms (residues 502−526, Å)	0.54 ± 0.14
rmsd of all heavy atoms (residues 502−526, Å)	1.05 ± 0.14
Overall (20 Structures)	
rmsd of backbone atoms (residues 502−526, Å)	0.76 ± 0.16
rmsd of all heavy atoms (residues 502−526, Å)	1.33 ± 0.15
mean deviations from ideal geometry	
bond length (Å)	0.001 86
bond angle (deg)	0.359

[a] A total of 11 structures belong to the first ensemble, and 9 structures belong to the second ensemble.

Description of the Structure of EosC2. Each conformer in Figure 4A contains a loose β hairpin that positions the two cysteinyl zinc ligands, followed by a short α helix, which contains the pair of zinc-ligating histidines. The length and nature of this α helix, which varies between four (Tyr518−Ser521) and seven residues (Tyr518−Val525) among the ensemble and the N-terminal portion (Tyr518−Ser521), is very well-ordered—φ angle order parameters are >0.99 for this region. The structures of EosC2 all display good covalent geometry (Table 1), and the root-mean-square deviation (rmsd) for a backbone overlay of the structured region (residues Arg502−Arg526) is 0.76 Å (Table 1). Residues His523−His529 appear mostly disordered because of the missing assignments in this region.

Interestingly, two distinct sets of conformers (blue and orange, referred to as EosC2′ and EosC2″, respectively; Figure 4A) are present within the ensemble of structures of EosC2. In parts B and C of Figure 4, the 20 lowest energy structures are separated according to which of the two conformers is taken up and the lowest energy structure from each ensemble is also shown as a ribbon diagram. Note that the lowest energy structure of EosC2 belonged to the EosC2″ (orange) set of conformers. These conformers differ in the region of the polypeptide backbone between the two zinc-ligating histidine residues, His523 and His529, and consequently in the arrangement of the zinc-ligation sphere. Analysis of the Ramachandran plot for each set of conformers revealed that the largest difference lay in the φ angle of Ser24 (φ_{24}); in all EosC2′ structures, φ_{24} was positive, whereas in all EosC2″ structures, φ_{24} was negative. Additional structure calculations in which φ_{24} was constrained to be either positive or negative confirmed that this angle is

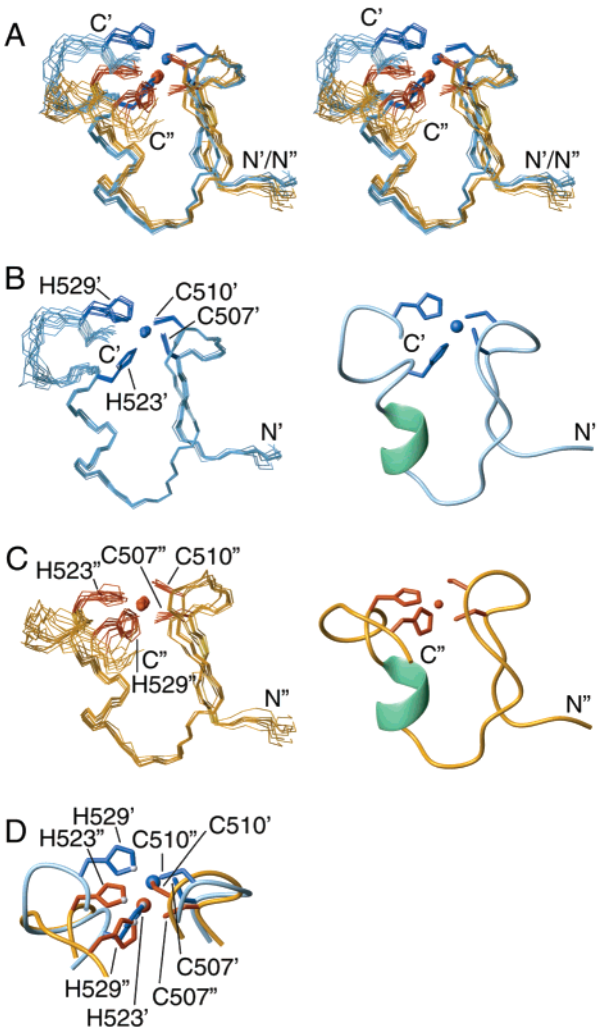

FIGURE 4: Solution structures of EosC2. (A) Ensemble of the 20 lowest energy solution structures of EosC2 calculated using ARIA 1.2 is shown in stereo. The two subfamilies of conformers present within this ensemble are shown in blue (EosC2′) and orange (EosC2″), and these structures are shown separately in B (EosC2′, 11 structures) and C (EosC2″, 9 structures), along with a ribbon diagram of the best structure for each set of conformers (the α helix recognized by MOLMOL is in green). The structures are superimposed for best fit over the backbone atoms of residues Arg502−Arg526, and the rmsd of these fits are 0.76, 0.34, and 0.54 Å in A, B, and C, respectively. For clarity, the unstructured residues (Phe501, Val531, and Gly532) are not displayed. The side chains of the zinc-ligating residues and the corresponding zinc ion are in dark blue or dark red and are labeled in B and C. The N and C termini are indicated. (D) Comparison of the zinc coordination sites of EosC2′ (blue) and EosC2″ (orange) is shown. The zinc-ligating residues are labeled, and the zinc-ligating atoms in His523 and His529 are shown as gray spheres.

a major determinant of which conformation is adopted. It is notable that His523−His529 is the region of the sequence that proved difficult to assign and which gave rise to broadened, absent, or duplicated resonances. Our favored interpretation is that the exchange process observed in the NMR spectra results from the two sets of conformers.

EosC2′ and EosC2″ Differ at the Zinc-Binding Site. The most striking difference between the two conformations of EosC2 occurs at the zinc-binding site. In Figure 4D, the side chains of the zinc-ligating residues are shown. Although the side chains of the equivalent cysteine residue from each conformation are in approximately the same position, the

positions of the side chains of His523′ and His529′ are switched compared with His523″ and His529″. This switch has the effect of inverting the chirality of the zinc-binding site. According to the convention described by Berg (*51*), EosC2′ has an *S* configuration, which is the same as that found in all other classical zinc fingers, while EosC2″ has an *R* configuration. This difference results in two distinct conformations for the C-terminal region of EosC2′ and EosC2″. In one conformation (blue; Figure 4B), the backbone completes another helix-like turn after His523′, adopts an extended conformation for residues Arg526′−Glu528′, and forms a small loop to position His529′ for zinc coordination. However, in the second conformer (Figure 4C), His529″ is placed in approximately the same position as His523′ by the backbone forming a large loop that runs roughly perpendicular to the long axis of the α helix.

Comparison with Classical ZnFs. Classical ZnFs can vary in the spacing between their zinc ligands. The two conformations of EosC2 were therefore compared with the structure of a classical ZnF that possessed an identical spacing of zinc ligands (i.e., $C-X_2-C-X_{12}-H-X_5-H$, where X is any amino acid), namely, the second ZnF from MBP-1 [MBP-1/2; PDB accession code 1BBO (*52*)]. In Figure 5A, it can be seen that the *β*-hairpin structure in the N-terminal half of MBP-1/2 is essentially maintained in EosC2′ and EosC2″, and an α helix is present in the C-terminal half of all three ZnFs. The major differences occur between EosC2″ and MBP-1/2 in the region that encompasses the zinc-ligating histidine residues. The position of the final two histidine residues in EosC2″ is swapped in comparison with the equivalent residues in MBP-1/2, which is accommodated by a dramatic change in the backbone conformation of EosC2″.

The residues that comprise the hydrophobic core of classical ZnFs are normally highly conserved (Figure 1). A comparison of the hydrophobic cores of EosC2″ (the lowest energy structure) and MBP-1/2 is shown in Figure 5B. Overall, the arrangement of the key residues is conserved. This is rather remarkable, given that the phenylalanine, which is usually present after the second zinc-ligating residue (Phe39 in MBP-1/2), is replaced by a serine in EosC2.

Examination of the Electrostatic Potential Surfaces of EosC1 and EosC2″. The electrostatic potential surfaces of EosC1 (the homology model) and EosC2″ (the lowest energy structure) were examined (parts C and D of Figure 5). It can be seen that no significant regions of positive charge are present, and this is consistent with the finding that EosC is not involved in DNA binding (*24*). The mixture of charges on the surfaces of EosC1 and EosC2″ is similar to the surface of the protein-binding classical ZnF from ATF-2 (*53*).

Alanine-Scanning Mutagenesis Reveals the Residues that Are Important for Oligomerization. After we determined the solution structure of EosC2, alanine-scanning mutagenesis was employed to establish which residues were responsible for mediating homo- and hetero-oligomerization. Mutants (M1−M21) were tested for their ability to interact with EosC (containing the Cys498Ser mutation introduced to minimize oxidation), as well as the C-terminal domains of Ikaros, Pegasus, and Trps1 (IkC, PegC, and Trps1C, respectively) in a yeast two-hybrid assay. All residues, except for glycine, zinc-ligating cysteine and histidine residues, and hydrophobic residues known to be important for the structure of classical ZnFs, were mutated pairwise to alanine (Figure 6A).

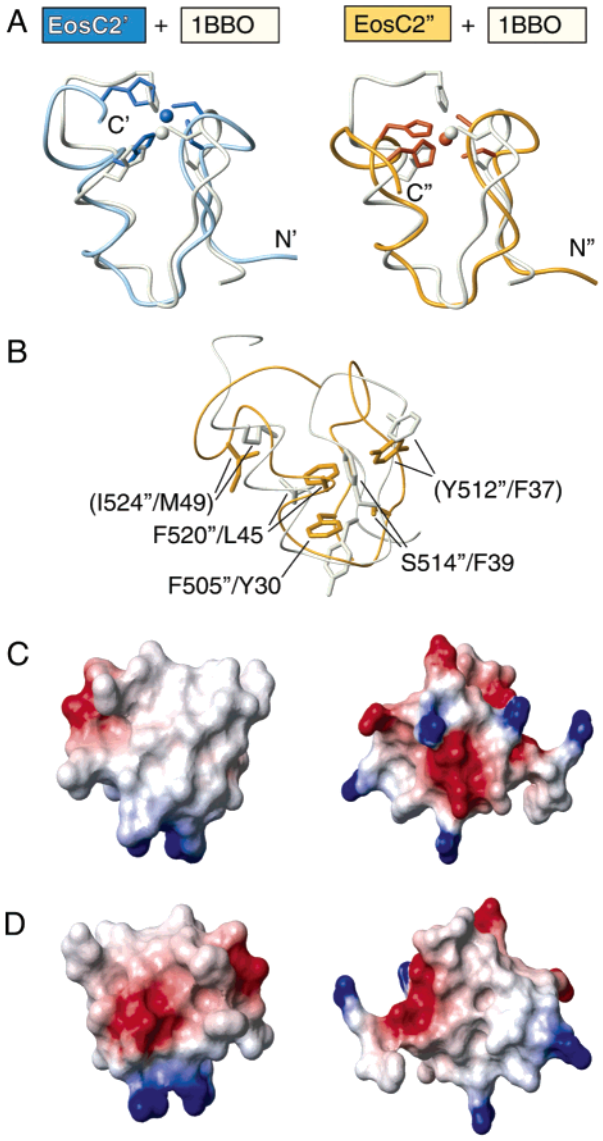

FIGURE 5: Comparison of the two conformations of EosC2 with classical ZnFs. (A) Lowest energy structures of EosC2′ (blue) and EosC2″ (orange) are shown as ribbon diagrams in the first and second columns, respectively, and are overlaid with MBP-1/2 (light yellow; PDB accession code 1BBO). The backbone atoms of residues between (and including) the second cysteine and the first histidine were used for the overlay (rmsd = 1.7 and 2.2 Å for EosC2′/1BBO and EosC2″/1BBO overlays, respectively). Only residues Arg502−Arg526 of the EosC2′/EosC2″ structures are shown. The zinc-ligating residues and Zn^{II} ions are colored appropriately. (B) Comparison of the hydrophobic cores from EosC2″ (orange) and MBP-1/2 (light yellow). The backbone traces, as well as the side chains of residues in MBP-1/2 that make up its hydrophobic core and the equivalent residues in EosC2″ are shown. In brackets are the residues that make up the hydrophobic core of MBP-1/2 but are not necessarily conserved among all classical ZnFs. (C and D) Electrostatic surface potentials of EosC1 (C) and EosC2″ (D) are shown. The left and right models are related by a 180° turn about a vertical axis in the plane of the page. Red = negative, blue = positive, and white = neutral.

The ability of M3, M6, M7, M8, M10, and M13 to interact with EosC was clearly impaired (Figure 6B). Similar results were obtained when the ability of the EosC mutants to hetero-oligomerize with IkC or PegC was tested, although some minor differences were observed (Figure 6B). Furthermore, all EosC mutants with the exception of M20 failed to interact strongly with Trps1C, suggesting that the EosC−Trps1C

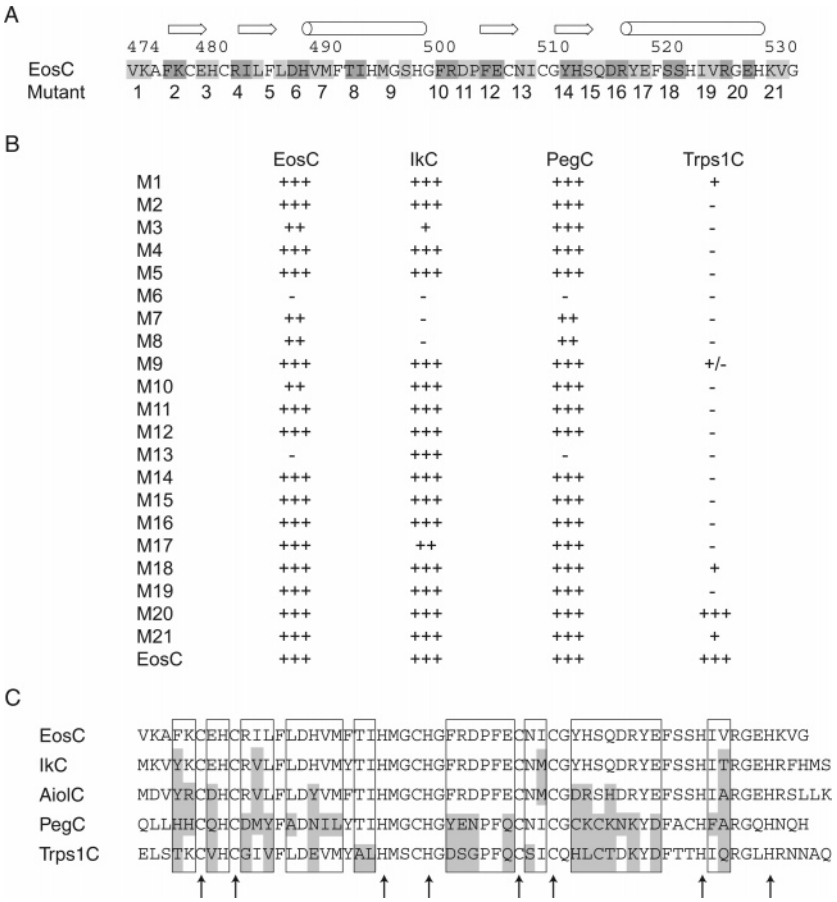

FIGURE 6: Alanine-scanning mutagenesis revealed residues that are important for EosC2 homo- and hetero-oligomerization. (A) Amino acids that were substituted with alanine (in a pairwise fashion) in M1−M21 are highlighted alternatively with light and dark gray. The numbering from full-length Eos is shown above the primary sequence. Typical secondary structural elements in classical ZnFs are indicated; arrows represent β strands, and cylinders indicate α helices. (B) Summary of the results obtained when mutants were tested for their ability to interact with EosC, IkC, PegC, and Trps1C in a yeast two-hybrid assay. Yeast growth is ranked from absent to strong (−, +, ++, and +++). EosC, IkC, PegC, and Trps1C were tested for their ability to auto-activate the histidine reporter gene (not shown) and to interact with EosC. (C) Sequence line up reveals the amino acid differences (gray) in IkC, AiolC, PegC, and Trps1C as compared with EosC. Only the differences that occur in regions found to be important for the interaction between EosC and Trps1C (boxed) are highlighted. Arrows indicate cysteine and histidine residues that are involved in zinc ligation.

interaction is highly specific and/or weaker than the other interactions. The specificity is consistent with our previously reported observation that IkC, AiolC, PegC, and Trps1C are not able to interact with Trps1C (*24*). A comparison of the primary sequences of these domains is shown in Figure 6C, where the positions of amino acids that appear to be important for the EosC−Trps1C interaction are boxed and deviations in IkC, AiolC, PegC, and Trps1C that occur at these positions (compared to EosC) are highlighted in gray. It is intriguing that IkC, although it contains only four changes compared to EosC within the boxed regions, is incapable of interacting with Trps1C, and this provides further evidence that the EosC−Trps1C interaction is highly specific.

To confirm that the lack of interaction observed with particular mutants was a consequence of disruption of a specific contact surface, rather than destabilization of the global structure, each mutant was checked for structural integrity by CD spectropolarimetry (Figure 7). M3, M7, M8, and M10 all fold in a zinc-dependent manner, similar to wild-type EosC (*24*). M6 and M13 could not be expressed in *Escherichia coli*, and it is possible that these mutants may not be folded correctly.

Identification of the Contact Surfaces in EosC Homo-oligomers. The three-dimensional positions of residues found

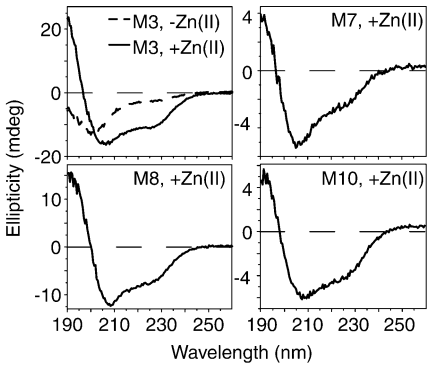

FIGURE 7: CD spectra of noninteracting mutants. The ability of noninteracting mutants to form secondary structure was monitored by CD. The spectrum recorded for M3 in the absence of Zn^{II} at a low pH is shown (- - -). M3, M7, M8, and M10 appear to successfully refold following the addition of Zn^{II} and an increase in pH (to ~5.3). The protein concentration in each sample was ~15 μM, and data were recorded at 25 °C.

to be important for EosC homo-oligomerization were examined using the homology model of EosC1 and the lowest energy structure of EosC2″; note that residues in EosC2 important for homo-oligomerization occur in the N-terminal region, which is essentially the same in both EosC2′ and

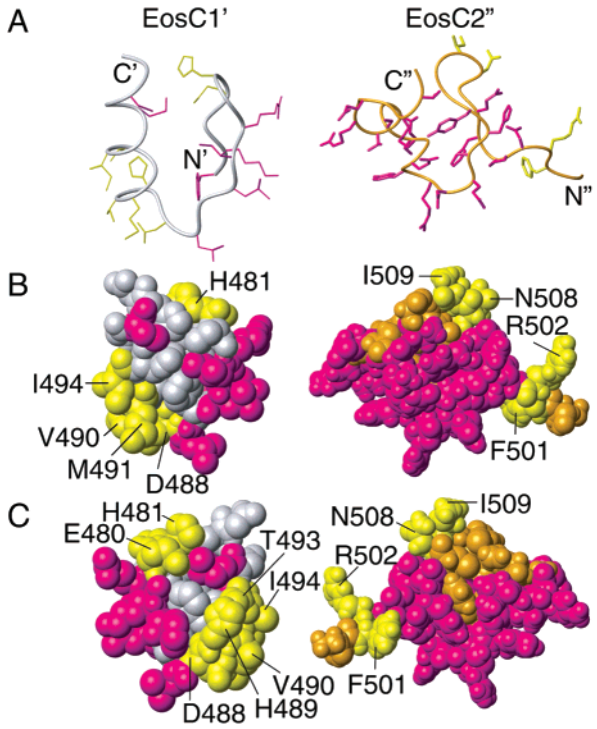

FIGURE 8: Probing the structure of EosC. (A) Structures of EosC1 (left) and EosC2″ (the lowest energy structure; right) are shown as ribbon models. (B) EosC1 and EosC2″ are shown as space-filling models, in the same orientation as in A, and models are rotated by 180° about a vertical axis in the plane of the page in C. In all models, the residues that were not targeted in the alanine scan are in light gray or orange for EosC1 or EosC2″, respectively, and residues that did not disrupt oligomerization are in magenta, while those that did are in yellow. The N and C termini are indicated in the ribbon diagrams.

EosC2″. Ribbon diagrams of EosC1 and EosC2″, along with the side chains that were targeted in the alanine scan, are shown in Figure 8A. The residues that when mutated to alanine did not disrupt oligomerization are in magenta, while those that did are in yellow. Space-filling models in the same orientation as the ribbon diagrams are in Figure 8B ("front" views), and the "back" views are in Figure 8C.

In an attempt to discern complementarity between EosC1 and EosC2″ that may reflect their relative orientations in the Eos oligomer, we used the protein-docking program HADDOCK (*42*). HADDOCK is a derivative of the NMR calculation package, ARIA, which uses information from experiments such as mutagenic screens to generate ambiguous intermolecular distance constraints. Different subsets of the mutants M3, M7, and M8 (in EosC1) were combined with M10 (in EosC2″) in a series of HADDOCK calculations, but no clear consensus structure was observed.

PegC1 and EosC2 Are Insufficient for Oligomerization. The results presented here indicate that the C-terminal domains of Eos and Pegasus consist of two autonomously folding, classical ZnF domains. Because the intact C-terminal domains of Eos and Pegasus have been shown to mediate homo- and heterotypic interactions (*11*), we sought to determine whether the single ZnFs were sufficient for these interactions. In the case of Ikaros, it has been shown that mutation of the zinc-ligating cysteine residues in either C-terminal ZnF results in the abrogation of homo-oligomerization [as tested in a yeast two-hybrid assay (*8*)], indicating that both ZnFs are required for these interactions. Sedimentation equilibrium data revealed that both PegC1 (not shown) and EosC2 (Figure 3C) are strictly monomeric in solution. Yeast two-hybrid experiments indicated that EosC1 is unable to interact with either itself or with EosC2, and this latter result was also confirmed by a combination of NMR titration data (not shown). These findings demonstrate that each ZnF domain is necessary but not sufficient for oligomerization and that a covalent link is required between the C1 and C2 domains for this process to take place.

DISCUSSION

It is clear that proteins in the Ikaros family of transcription factors are important for normal cellular development. However, despite the fact that Ikaros was first discovered over 10 years ago (*15*), the details of the molecular mechanisms of action of this family have remained elusive. Recent work in our laboratory revealed that the C-terminal double-ZnF domain of Eos mediates the formation of monodisperse oligomers containing 9 or 10 subunits (*24*), and in the current study, we sought to examine this domain at a more detailed level.

In a "divide-and-conquer" strategy, we have used several biophysical methods to characterize the structures of the two putative zinc-binding domains (C1 and C2) in the C-terminal region of Eos and Pegasus. CD, UV−vis, and NMR spectroscopic studies revealed that the two domains are each able to adopt zinc-binding folds independent of the other and that each fold resembles that of the classical ZnF.

NMR spectra of the C2 domain of Eos revealed the existence of a conformational exchange process involving the C-terminal third of the domain. The family of conformers calculated for EosC2 from the NMR data contained two subfamilies that differ substantially in the arrangement of the protein chain at the C terminus. In particular, the spatial arrangement of the two histidine side chains that ligate the Zn^{II} ion is reversed in the different conformers. Interconversion between these two conformers would probably require dissociation of the two histidine ligands from the Zn^{II}. Interestingly, we have recently observed metal exchange taking place on a millisecond to second time scale in a classical ZnF. Such a time scale is consistent with the chemical exchange broadening observed in our spectra. It should be noted that because relatively few experimental constraints were observed for residues in this region of the protein, the observed conformers may not reflect the precise nature of the exchange process. Nevertheless, our principal conclusion that a substantial degree of conformational flexibility exists in EosC2 is accurate.

This is an intriguing result, given the common view that classical ZnFs are compact, well-ordered structures. Potentially, EosC2 may take up a better-defined structure by packing against EosC1 and/or the formation of the oligomeric state. Recently, it was reported that the conformation of one of the ZnFs from the transcription factor MTF-1 (*54*), which contains six classical ZnFs, is also dynamic (*54*). Selective broadening in NMR spectra of MTF-1 led to the finding that the fifth ZnF undergoes conformational exchange that is highly dependent upon the zinc concentration. The conformational exchange occurred even in the presence of the flanking ZnFs (ZnFs 4 and 6), presenting the possibility that the dynamic behavior observed for EosC2 might occur even

in the context of intact Eos. Thus, conformational instability may be relatively common among zinc-binding domains.

Another notable feature of the structure of EosC2 was the arrangement of the hydrophobic core (Figure 5B), which was well-defined, despite the absence of the phenylalanine residue (four positions after the second cysteine; Figure 1) that is generally taken as one of the invariant residues in classical ZnFs. This residue is substituted by serine in EosC2, and the loss of the bulky hydrophobic amino acid appears to be compensated by both the substitution of a normally conserved leucine for phenylalanine (Figure 1) and the repositioning of Phe505 and Tyr512 closer to the center of the core. Interestingly, it is possible that the substitution of Ser514 for the conserved phenylalanine in EosC2 contributes to the conformational exchange observed for this single ZnF; studies on another classical ZnF (from ZFY) revealed that replacement of this conserved phenylalanine residue with a leucine similarly leads to a more dynamic structure (*55*).

Alanine-scanning mutagenesis revealed that at least four pairs of amino acids are important for the oligomerization of EosC. Two additional pairs of amino acids (Asp488, His489 and Asn508, Ile509) may also play a role in the interaction, although our inability to recombinantly express domains with mutations at these positions implies that these residues are instead involved in maintaining the structural integrity of EosC. The latter possibility, if true, would indicate that the structural requirements of EosC might deviate substantially from those of other classical ZnFs.

Other groups have identified residues in IkC that are important for oligomerization (*8*, *56*). Generally, our results corroborate those from McCarty and co-workers, indicating that the N-terminal end of the α helix in the first ZnF of EosC (Figure 6A) and IkC is important for homo-oligomerization, although the results of Sun and co-workers are not completely consistent with this conclusion. There are also discrepancies regarding which residues in the second ZnF are required for oligomerization. It is notable that the effects of mutations on the structural integrity of IkC were not tested, and it is therefore possible that some of the residues identified in IkC as being important for self-association are instead required for structural integrity.

Examination of the electrostatic surface potentials of EosC1 and EosC2 revealed that neither ZnF possesses the extensive positively charged region that is common in DNA-binding ZnFs. The mixture of charges present on the surfaces of EosC1 and EosC2 may reflect the higher level of complexity required by ZnFs to bind to other proteins rather than to bind to the regular, negatively charged structure of DNA. Differences such as this may prove to be useful criteria in distinguishing protein binding from DNA-binding ZnFs on the basis of amino acid sequence.

Finally, a combination of yeast two-hybrid and biophysical experiments demonstrated that neither of the single C-terminal ZnFs is capable of associating either with itself or with the other ZnF. Thus, the double-ZnF domain is strictly required for homo-oligomerization, as reported previously for Ikaros (*8*). It is worthwhile to note that the linker between the C-terminal ZnFs is different from the highly conserved linker (TGEKP) that normally occurs between classical, DNA-binding ZnFs (*57*). This linker region may play a role in the self-association of Ikaros-family proteins.

In summary, we have sought to address the lack of structural information on Ikaros-family proteins, which is due in large part to the poor solution properties of each of the isolated ZnFs and of the intact C-terminal domain. The solution structure of EosC2 has revealed both similarities and differences to other classical ZnFs, and site-directed mutagenesis has allowed us to define the amino acids required for both the self-association and hetero-oligomerization of Eos.

REFERENCES

1. Mackay, J. P., and Crossley, M. (1998) *Trends Biochem. Sci. 23*, 1−4.
2. Wolfe, S. A., Nekludova, L., and Pabo, C. O. (2000) *Annu. Rev. Biophys. Biomol. Struct. 29*, 183−212.
3. Zhou, Q., Gedrich, R. W., and Engel, D. A. (1995) *J. Virol. 69*, 4323−4330.
4. Merika, M., and Orkin, S. H. (1995) *Mol. Cell. Biol. 15*, 2437−2447.
5. Lee, J. S., Galvin, K. M., and Shi, Y. (1993) *Proc. Natl. Acad. Sci. U.S.A. 90*, 6145−6149.
6. Lee, J. S., See, R. H., Galvin, K. M., Wang, J., and Shi, Y. (1995) *Nucleic Acids Res. 23*, 925−931.
7. Kalenik, J. L., Chen, D., Bradley, M. E., Chen, S. J., and Lee, T. C. (1997) *Nucleic Acids Res. 25*, 843−849.
8. Sun, L., Liu, A., and Georgopoulos, K. (1996) *EMBO J. 15*, 5358−5369.
9. Molnar, A., and Georgopoulos, K. (1994) *Mol. Cell. Biol. 14*, 8292−8303.
10. Morgan, B., Sun, L., Avitahl, N., Andrikopoulos, K., Ikeda, T., Gonzales, E., Wu, P., Neben, S., and Georgopoulos, K. (1997) *EMBO J. 16*, 2004−2013.
11. Perdomo, J., Holmes, M., Chong, B., and Crossley, M. (2000) *J. Biol. Chem. 275*, 38347−38354.
12. Hahm, K., Cobb, B. S., McCarty, A. S., Brown, K. E., Klug, C. A., Lee, R., Akashi, K., Weissman, I. L., Fisher, A. G., and Smale, S. T. (1998) *Genes Dev. 12*, 782−796.
13. Honma, Y., Kiyosawa, H., Mori, T., Oguri, A., Nikaido, T., Kanazawa, K., Tojo, M., Takeda, J., Tanno, Y., Yokoya, S., Kawabata, I., Ikeda, H., and Wanaka, A. (1999) *FEBS Lett. 447*, 76−80.
14. Kelley, C. M., Ikeda, T., Koipally, J., Avitahl, N., Wu, L., Georgopoulos, K., and Morgan, B. A. (1998) *Curr. Biol. 8*, 508−515.
15. Georgopoulos, K., Moore, D. D., and Derfler, B. (1992) *Science 258*, 808−812.
16. Klug, C. A., Morrison, S. J., Masek, M., Hahm, K., Smale, S. T., and Weissman, I. L. (1998) *Proc. Natl. Acad. Sci. U.S.A. 95*, 657−662.
17. Georgopoulos, K., Bigby, M., Wang, J. H., Molnar, A., Wu, P., Winandy, S., and Sharpe, A. (1994) *Cell 79*, 143−156.
18. Nakase, K., Ishimaru, F., Fujii, K., Tabayashi, T., Kozuka, T., Sezaki, N., Matsuo, Y., and Harada, M. (2002) *Exp. Hematol. 30*, 313−317.
19. Hosokawa, Y., Maeda, Y., Takahashi, E., Suzuki, M., and Seto, M. (1999) *Genomics 61*, 326−329.
20. Cortes, M., and Georgopoulos, K. (2004) *J. Exp. Med. 199*, 209−219.
21. Georgopoulos, K., Winandy, S., and Avitahl, N. (1997) *Annu. Rev. Immunol. 15*, 155−176.
22. Wang, J. H., Avitahl, N., Cariappa, A., Friedrich, C., Ikeda, T., Renold, A., Andrikopoulos, K., Liang, L., Pillai, S., Morgan, B. A., and Georgopoulos, K. (1998) *Immunity 9*, 543−553.
23. Momeni, P., Glockner, G., Schmidt, O., von Holtum, D., Albrecht, B., Gillessen-Kaesbach, G., Hennekam, R., Meinecke, P., Zabel, B., Rosenthal, A., Horsthemke, B., and Ludecke, H. J. (2000) *Nat. Genet. 24*, 71−74.
24. Westman, B. J., Perdomo, J., Sunde, M., Crossley, M., and Mackay, J. P. (2003) *J. Biol. Chem. 278*, 42419−42426.
25. Haire, R. N., Miracle, A. L., Rast, J. P., and Litman, G. W. (2000) *J. Immunol. 165*, 306−312.
26. Molnar, A., Wu, P., Largespada, D. A., Vortkamp, A., Scherer, S., Copeland, N. G., Jenkins, N. A., Bruns, G., and Georgopoulos, K. (1996) *J. Immunol. 156*, 585−592.

27. Mackay, J. P., Kowalski, K., Fox, A. H., Czolij, R., King, G. F., and Crossley, M. (1998) *J. Biol. Chem. 273*, 30560−30567.
28. Johnson, M. L., Correia, J. J., Yphantis, D. A., and Halvorson, H. R. (1981) *Biophys. J. 36*, 575−588.
29. Hayes, D. B., Laue, T., and Philo, J. (1995) *SEDNTERP*, University of New Hampshire, Durham, NH.
30. Bartels, C., Xia, T.-H., Billeter, P., Guntert, P., and Wuthrich, K. (1995) *J. Biomol. NMR 5*, 1−10.
31. Guntert, P., Mumenthaler, C., and Wuthrich, K. (1997) *J. Mol. Biol. 273*, 283−298.
32. Nilges, M. (1995) *J. Mol. Biol. 245*, 645−660.
33. Nilges, M., Macias, M. J., O'Donoghue, S. I., and Oschkinat, H. (1997) *J. Mol. Biol. 269*, 408−422.
34. Brunger, A. T., Adams, P. D., Clore, G. M., DeLano, W. L., Gros, P., Grosse-Kunstleve, R. W., Jiang, J. S., Kuszewski, J., Nilges, M., and Pannu, N. S., et al. (1998) *Acta Crystallogr., Sect. D 54* (Part 5), 905−921.
35. Neuhaus, D., Nakaseko, Y., Schwabe, J. W., and Klug, A. (1992) *J. Mol. Biol. 228*, 637−651.
36. Linge, J. P., and Nilges, M. (1999) *J Biomol. NMR 13*, 51−59.
37. Folmer, R. H., Hilbers, C. W., Konings, R. N., and Nilges, M. (1997) *J. Biomol. NMR 9*, 245−258.
38. Koradi, R., Billeter, M., and Wuthrich, K. (1996) *J. Mol. Graphics 14*, 51−55.
39. Laskowski, R. A., Rullmannn, J. A., MacArthur, M. W., Kaptein, R., and Thornton, J. M. (1996) *J. Biomol. NMR 8*, 477−486.
40. Guex, N., Diemand, A., and Peitsch, M. C. (1999) *Trends Biochem. Sci. 24*, 364−367.
41. Guex, N., and Peitsch, M. C. (1997) *Electrophoresis 18*, 2714−2723.
42. Dominguez, C., Boelens, R., and Bonvin, A. M. (2003) *J. Am. Chem. Soc. 125*, 1731−1737.
43. Hubbard, S. J., and Thornton, J. M. (1993) Department of Biochemistry and Molecular Biology, University College, London, U.K.
44. Frankel, A. D., Berg, J. M., and Pabo, C. O. (1987) *Proc. Natl. Acad. Sci. U.S.A. 84*, 4841−4845.
45. Burke, C. J., Sanyal, G., Bruner, M. W., Ryan, J. A., LaFemina, R. L., Robbins, H. L., Zeft, A. S., Middaugh, C. R., and Cordingley, M. G. (1992) *J. Biol. Chem. 267*, 9639−9644.
46. Michael, S. F., Kilfoil, V. J., Schmidt, M. H., Amann, B. T., and Berg, J. M. (1992) *Proc. Natl. Acad. Sci. U.S.A. 89*, 4796−4800.
47. Bertini, I., and Luchinat, C. (1984) *Adv. Inorg. Biochem. 6*, 71−111.
48. Simpson, R. J., Cram, E. D., Czolij, R., Matthews, J. M., Crossley, M., and Mackay, J. P. (2003) *J. Biol. Chem. 278*, 28011−28018.
49. Wishart, D. S., Sykes, B. D., and Richards, F. M. (1992) *Biochemistry 31*, 1647−1651.
50. Wishart, D. S., and Sykes, B. D. (1994) *J. Biomol. NMR 4*, 171−180.
51. Berg, J. M. (1988) *Proc. Natl. Acad. Sci. U.S.A. 85*, 99−102.
52. Omichinski, J. G., Clore, G. M., Robien, M., Sakaguchi, K., Appella, E., and Gronenborn, A. M. (1992) *Biochemistry (Moscow) 31*, 3907−3917.
53. Nagadoi, A., Nakazawa, K., Uda, H., Okuno, K., Maekawa, T., Ishii, S., and Nishimura, Y. (1999) *J. Mol. Biol. 287*, 593−607.
54. Giedroc, D. P., Chen, X., Pennella, M. A., and LiWang, A. C. (2001) *J. Biol. Chem. 276*, 42322−42332.
55. Lachenmann, M. J., Ladbury, J. E., Phillips, N. B., Narayana, N., Qian, X., and Weiss, M. A. (2002) *J. Mol. Biol. 316*, 969−989.
56. McCarty, A. S., Kleiger, G., Eisenberg, D., and Smale, S. T. (2003) *Mol. Cell 11*, 459−470.
57. Laity, J. H., Dyson, H. J., and Wright, P. E. (2000) *J. Mol. Biol. 295*, 719−727.

BI049506A